priate source-shape corrections. The spatial resolution can be improved by using smaller apertures and through waveguide focusing effects, if it is not intensity-limited by the detectable maximum momentum transfer. When reducing the size of the reference aperture, either the X-ray transmission of the sample or the sample aperture size may have to be reduced to control the relative sample and reference beam intensities. If a reference beam intensity larger than the sample beam intensity cannot be achieved, nonlinearities in the holographic imaging process will have to be taken into account. A relative drift of the mask–sample structure relative to the CCD detector is not critical as long as it is smaller than the CCD pixel size (13.5 μm). Vibration isolation and thermal stabilization is therefore easy in comparison with other submicrometre microscopy techniques. Furthermore, extreme sample environments such as high magnetic fields or low temperatures can easily be implemented because there are no stringent space constraints around the sample.

Another exciting possibility is an improvement in spatial resolution by application of iterative phase retrieval methods[2,8,9,25] to the hologram. Our mask-based X-ray Fourier transform holography approach is fully compatible with iterative phase retrieval, provided that the hologram is recorded with sufficient resolution. In a combined approach we record a high-resolution X-ray hologram and the holographic image obtained by Fourier transformation is then used as the starting point for iterative refinement of the phase. In this way, ambiguities in the iterative process are restricted to the finest details of the image below the resolution of the holographic image. The ultimate resolution is then determined not by the reference pinhole size but by the maximum photon momentum transfer or, eventually, by the wavelength.

The present work was in part motivated by the expected availability of X-ray free-electron lasers in the near future[26,27]. Such sources will provide coherent high-intensity X-ray pulses of femtosecond duration. From the exposure time and coherent flux used for our images we can estimate that a single X-ray free-electron laser pulse will be sufficient to record an ultrafast single shot image. This will open the door for taking ultrafast movies of processes on the nanometre length scale, for example, of phase transitions. Our holographic approach is well matched to the spatial and temporal source properties of a free-electron laser and is the method of choice for single-shot ultrafast imaging with such sources[4]. □

Methods

Soft X-rays with circular polarization are generated in a APPLE-II-type helical undulator with 30 periods of length 56 mm. An energy resolution of $\lambda/\Delta\lambda = 2{,}000$ was obtained with a spherical grating monochromator. The 20-μm diameter aperture used for spatial filtering was located 6 m downstream of the beamline focus, thus accepting approximately 0.1% of the total beamline photon flux. Holograms were recorded with a Princeton Instruments PI-SX CCD camera equipped with an in-vacuum back-illuminated chip of 2,048 × 2,048 pixels of width 13.5 μm. For the hologram shown in Fig. 2, about 1×10^{10} photons were incident on the CCD chip during the accumulated exposure time. The apertures of the Fourier transform holography mask were prepared with a dual-beam focused ion beam instrument from FEI (Strata 235). The scanning X-ray microscopy image was recorded on the microscopy station on beamline 11 at the Advanced Light Source, Berkeley. The microscope has been described by ref. 19.

Received 8 July; accepted 28 October 2004; doi:10.1038/nature03139.

1. Stroke, G. W. *An Introduction to Coherent Optics and Holography* (Academic, New York, 1969).
2. Miao, J. W., Charalambous, P., Kirz, J. & Sayre, D. Extending the methodology of X-ray crystallography to allow imaging of micrometre-sized non-crystalline specimens. *Nature* **400,** 342–344 (1999).
3. Chao, W. L. *et al.* 20-nm-resolution soft x-ray microscopy demonstrated by use of multilayer test structures. *Opt. Lett.* **28,** 2019–2021 (2003).
4. Neutze, R., Wouts, R., Van der Spoel, D., Weckert, E. & Hajdu, J. Potential for biomolecular imaging with femtosecond X-ray pulses. *Nature* **406,** 752–757 (2000).
5. Ade, H. & Hsiao, B. X-ray linear dichroism microscopy. *Science* **262,** 1427–1429 (1993).
6. Stöhr, J. *et al.* Element-specific magnetic microscopy with circularly polarized X-rays. *Science* **259,** 658–661 (1993).
7. Fischer, P. *et al.* Magnetic domain imaging with a transmission X-ray microscope. *J. Magn. Magn. Mater.* **199,** 624–627 (1999).
8. Gerchberg, R. W. & Saxton, W. O. Practical algorithm for determination of phase from image and diffraction plane pictures. *Optik* **35,** 237–246 (1972).
9. Fienup, J. R. Phase retrieval algorithms—a comparison. *Appl. Opt.* **21,** 2758–2769 (1982).
10. Gabor, D., Kock, W. E. & Stroke, G. W. Holography. *Science* **173,** 11–23 (1971).
11. Focus on X-ray microscopy. *Synchrotron Radiat. News* (special issue, ed. Schmahl, G.) **16**(3), 2–63 (2003).
12. Stöhr, J. *et al.* Element-specific magnetic microscopy with circularly polarized X-rays. *Science* **259,** 658–661 (1993).
13. Xu, W. B., Jericho, M. H., Meinertzhagen, I. A. & Kreuzer, H. J. Digital in-line holography for biological applications. *Proc. Natl Acad. Sci. USA* **98,** 11301–11305 (2001).
14. Trebes, J. E. *et al.* Demonstration of X-ray holography with an X-ray laser. *Science* **238,** 517–519 (1987).
15. McNulty, I. *et al.* High-resolution imaging by Fourier-transform X-ray holography. *Science* **256,** 1009–1012 (1992).
16. Lindaas, S., Howells, H., Jacobsen, C. & Kalinovsky, A. X-ray holographic microscopy by means of photoresist recording and atomic-force microscope readout. *J. Opt. Soc. Am. A Opt. Image Sci. Vis.* **13,** 1788–1800 (1996).
17. Hannon, J. P., Trammell, G. T., Blume, M. & Gibbs, D. X-ray resonance exchange scattering. *Phys. Rev. Lett.* **61,** 1245–1248 (1988).
18. Hellwig, O., Denbeaux, G. P., Kortright, J. B. & Fullerton, E. E. X-ray studies of aligned magnetic stripe domains in perpendicular multilayers. *Physica B Condens. Matter* **336,** 136–144 (2003).
19. Kilcoyne, A. L. D. *et al.* Interferometer-controlled scanning transmission X-ray microscopes at the Advanced Light Source. *J. Synchrotron Radiat.* **10,** 125–136 (2003).
20. Stroke, G. W. Lensless Fourier-transform method for optical holography. *Appl. Phys. Lett.* **6,** 201–203 (1965).
21. Winthrop, J. T. & Worthing, C. R. X-ray microscopy by successive Fourier transformation. *Phys. Lett.* **15,** 124–126 (1965).
22. Kortright, J. B. *et al.* Soft-x-ray small-angle scattering as a sensitive probe of magnetic and charge heterogeneity. *Phys. Rev. B* **64,** 92401 (2001).
23. Eisebitt, S. *et al.* Polarization effects in coherent scattering from magnetic specimen: Implications for x-ray holography, lensless imaging, and correlation spectroscopy. *Phys. Rev. B* **68,** 104419 (2003).
24. Bergemann, C., Keymeulen, H. & Van der Veen, J. F. Focusing X-ray beams to nanometer dimensions. *Phys. Rev. Lett.* **91,** 204801 (2003).
25. Fienup, J. R. Reconstruction of a complex-valued object from the modulus of its Fourier transform using a support constraint. *J. Opt. Soc. Am.* **4,** 118–123 (1987).
26. Cho, A. The ultimate bright idea. *Science* **296,** 1008–1010 (2002).
27. Emma, P. *et al.* Femtosecond and subfemtosecond X-ray pulses from a self-amplified spontaneous-emission–based free-electron laser. *Phys. Rev. Lett.* **92,** 074801 (2004).

Acknowledgements We thank Y. Acremann for recording the STXM image of the sample at the Advanced Light Source and E. E. Fullerton for access to his thin film deposition facility. The work of the SSRL authors is supported by the US Department of Energy, Office of Basic Energy Sciences.

Competing interests statement The authors declare that they have no competing financial interests.

Correspondence and requests for materials should be addressed to S.E. (eisebitt@bessy.de) or J.L. (luning@stanford.edu).

High temperatures in the Late Cretaceous Arctic Ocean

Hugh C. Jenkyns[1], Astrid Forster[2], Stefan Schouten[2] & Jaap S. Sinninghe Damsté[2]

[1]*Department of Earth Sciences, University of Oxford, Parks Road, Oxford OX1 3PR, UK*
[2]*Royal Netherlands Institute for Sea Research (NIOZ), Department of Marine Biogeochemistry and Toxicology, PO Box 59, 1790 AB Den Burg, Texel, The Netherlands*

To understand the climate dynamics of the warm, equable greenhouse world of the Late Cretaceous period, it is important to determine polar palaeotemperatures. The early palaeoceanographic history of the Arctic Ocean has, however, remained largely unknown, because the sea floor and underlying deposits are usually inaccessible beneath a cover of floating ice. A shallow piston core taken from a drifting ice island in 1970 fortuitously retrieved unconsolidated Upper Cretaceous organic-rich sediment from Alpha ridge[1–4], a submarine elevated feature of probable oceanic origin[5]. A lack of carbonate in the sediments from this core has prevented the use of traditional oxygen-isotope palaeothermometry. Here we determine Arctic palaeotemperatures from these Upper Cretaceous deposits using TEX_{86},

a new palaeothermometer that is based on the composition of membrane lipids derived from a ubiquitous component of marine plankton, Crenarchaeota[6]. From these analyses we infer an average sea surface temperature of ~15 °C for the Arctic Ocean about 70 million years ago[7]. This calibration point implies an Equator-to-pole gradient in sea surface temperatures of ~15 °C during this interval and, by extrapolation, we suggest that polar waters were generally warmer than 20 °C during the middle Cretaceous (~90 million years ago).

Only three cores containing well-dated Cretaceous deep-sea sediment are known from the Arctic Ocean. The piston cores Fl-437 and Fl-533 were taken during the drift of the Arctic ice island T-3 (Fletcher's ice island) over Alpha ridge (Fig. 1) during the period 1963–74. Fl-437, cored in 1969, comprises yellowish laminated siliceous ooze rich in exquisitely preserved diatoms (*Anualus*, *Hemiaulus* and *Rhizosolenia* being the most abundant genera in a low-diversity assemblage), with subsidiary ebridians, silicoflagellates, archaeomonads and sparse fish remains: the initial age attribution of mid- to late Maastrichtian[1] has now been extended to include the Campanian[8]. Core 6 of the Canadian Expedition to Study the Alpha Ridge (CESAR), taken in 1983 from a research station installed on drifting sea ice (Fig. 1), is composed of siliceous sediments very similar to those of core Fl-437, being spectacularly laminated on a millimetre scale and similarly lacking planktonic carbonate[1,3,9]. Total organic carbon (TOC) contents in these sediments are low, typically <1% (ref. 3). The age attribution of this core includes the interval Campanian–Maastrichtian, depending on whether the diatoms, the silicoflagellates or the palynomorphs are taken as the prime biostratigraphic indicator[10–12].

Fl-533, cored in 1970, comprises homogeneous (apart from a finely laminated uppermost 2 cm) organic-rich black mud whose TOC content ranges between 11.0 and 15.8 wt% (Fig. 2). The organic matter comprises amorphous material, abundant woody fragments, leaf cuticles, spores and pollen; marine dinoflagellates are particularly abundant[2]. Hydrogen indices (150–350 mg hydrocarbons per g organic carbon) equally suggest the presence of marine and terrestrial components, a conclusion consistent with the presence of marine and terrestrial biomarkers. Our analyses indicate that biomarkers derived from diatoms are abundant in these deposits even though their siliceous frustules are not recorded, presumably because they have dissolved within the sediment: the C_{25} highly branched isoprenoid is derived from centric diatoms of the order *Rhizosolenia* and indicates an age younger than Turonian, the period in which these forms evolved[13]. The relative abundance of 24-norcholestanes, a group of steroids, is also diagnostic because their occurrence is generally associated with high-latitude deposition of diatomaceous ooze[14]. Initially dated as late Campanian or late Campanian to Maastrichtian[1,2], re-examination of the dinoflagellate cysts, together with acritarchs and prasinophytes, suggests an early Maastrichtian age for these black muds[4].

Integration of these various biostratigraphic indices from all three Upper Cretaceous sections allows more than one interpretation: the organic-rich and siliceous sediments could either be coeval or represent successive episodes of pelagic deposition (Fig. 2).

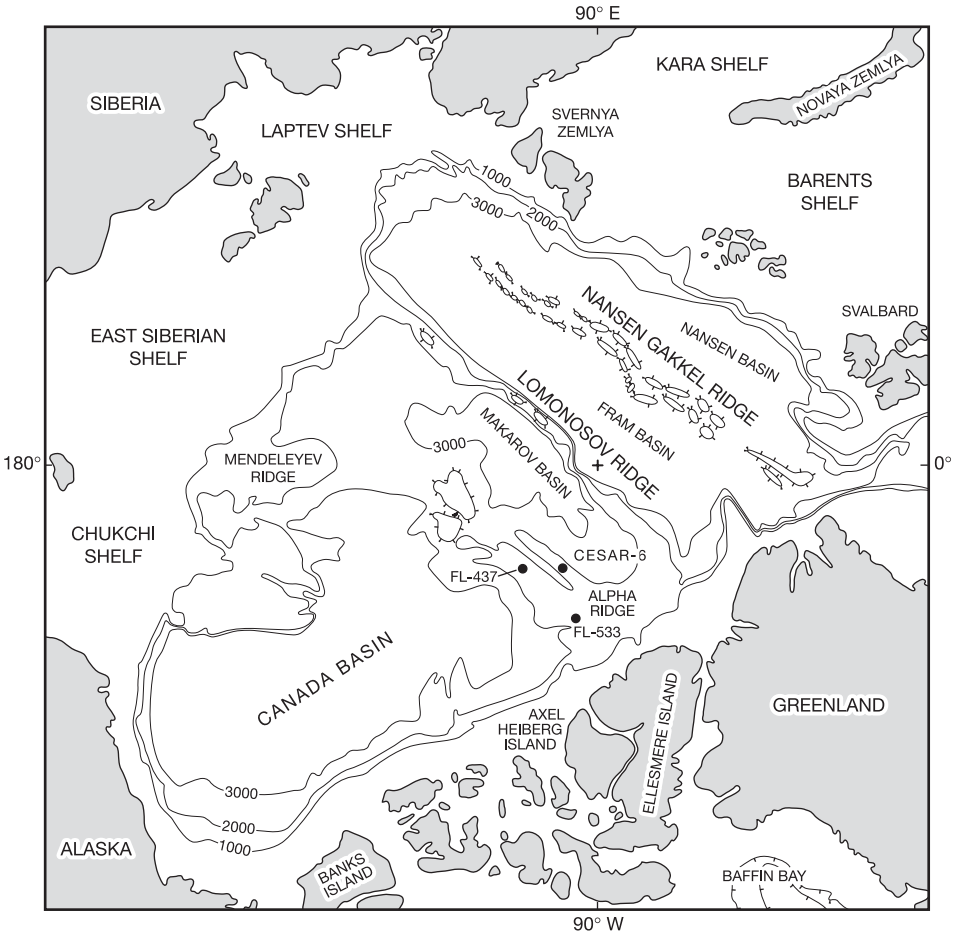

Figure 1 Map of the Arctic Ocean. Also shown (filled circles) are the locations of the three sites on the Alpha ridge where Cretaceous sediments have been retrieved. Core Fl-533, containing 67 cm of black mud, was cored at a water depth of 1,855 m on the eastern end of the structure (85° 05.9′ N, 98° 17.8′ W). Modified from ref. 9.

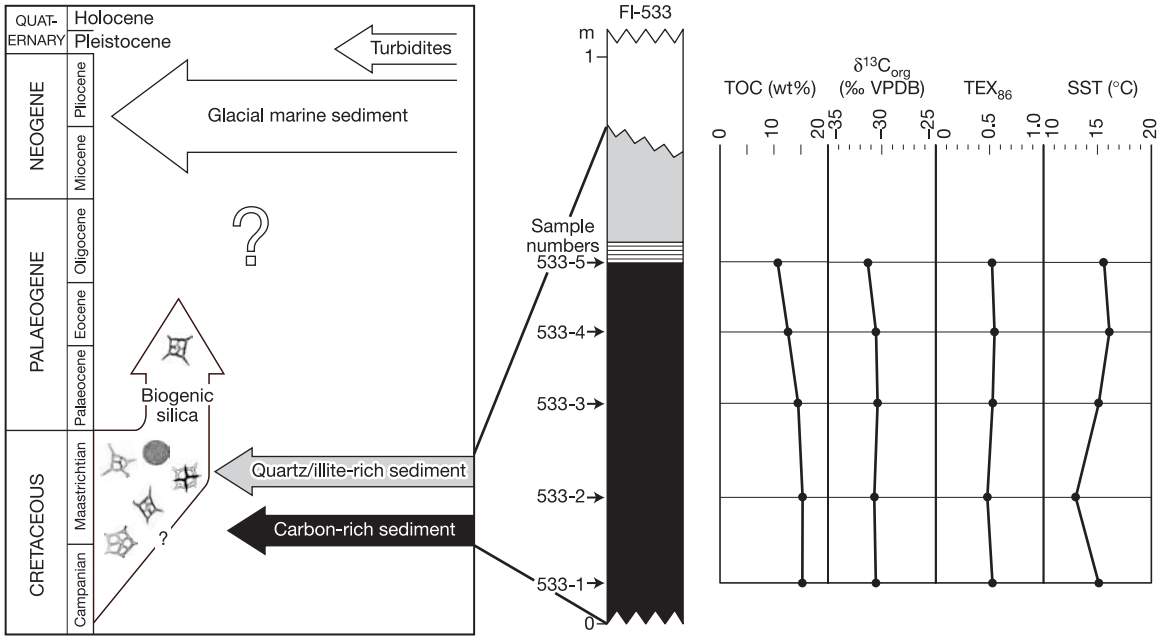

Figure 2 Suggested stratigraphic relationships of Campanian–Maastrichtian biogenic sediments of the Alpha ridge, Arctic Ocean. Our organic geochemical data from the black muds are shown against the lithological log for core Fl-533. Stratigraphy modified from ref. 1 to incorporate the more recent data of ref. 4. Sea surface temperature (SST), using the TEX_{86} parameter, calculated after the methodology given in refs 6, 16 and this Letter. TOC, total organic carbon.

Both sediments can be interpreted as the product of open-marine fertile waters, probably influenced by active upwelling centres that may have varied, with respect to their nutrient concentrations and planktonic biota, in time and space[4,8,15]. Diatoms, however, were clearly a significant part of the biota when both siliceous and organic-rich sediments were accumulating, even though they have apparently left no obvious hard parts in the black muds. Strong seasonality is implied by the laminated varve-like nature of the siliceous sediments, with layers rich in resting spores of diatoms alternating with layers rich in their vegetative cells. The remarkably pristine state of preservation of the siliceous biota in cores Fl-437 and CESAR-6 and the thermal immaturity of the marine organic matter (predominance (>80%) of ββ-homohopane isomers) in core Fl-533 implies minimal diagenesis, presumably a function of the lack of sedimentary overburden. There are no dropstones in any of these sediments, so there is a complete lack of evidence for glacial activity.

Because the paucity of biogenic carbonate ($CaCO_3$ contents are <1% in the black muds[2]) in the sediments of all three cores precludes application of the oxygen-isotope palaeothermometer, we analysed five samples of the black shale from core Fl-533 for membrane lipids of marine Crenarchaeota to determine the TEX_{86} ('tetraether index of 86 carbon atoms') parameter[6]. Marine Crenarchaeota are ubiquitous microorganisms that make up 20–30% of the picoplankton in present-day oceans, and their molecular fossils have been found in immature organic-rich sediments as old as Aptian (Early Cretaceous)[16]. Studies on marine core-top sediments have shown a significant ($r^2 = 0.92$) correlation between the number of cyclopentane rings in these lipids and annual mean sea surface temperature[6]. Furthermore, analysis of Cretaceous Atlantic black shales, using the TEX_{86} parameter, gave results that show excellent correlation with palaeotemperatures derived from $\delta^{18}O$ values of well-preserved glassy planktonic foraminifera[16]. The results of our analyses, shown in Fig. 2, indicate average Arctic Ocean (~80° N) sea surface temperatures of 15 ± 1 °C for that part of the early Maastrichtian represented by the black muds.

The data presented here allow determination of the climatic gradient during the Late Cretaceous, commonly considered to be particularly subdued with respect to that of the present day[17,18]. Oxygen-isotope data from Maastrichtian (probably early to mid-Maastrichtian) primary skeletal aragonite and enclosing magnesian-calcite cements deriving from a drowned carbonate platform (guyot) in the western Pacific indicate palaeo-equatorial (~5–10° S) temperatures of ~27–32 °C (ref. 19). Thus, assuming no rapid global climatic change during the early to mid-Maastrichtian—oxygen-isotope data from most sites in the world ocean imply a gradual surface-water cooling during this interval[18]—an Equator-to-pole gradient of ~15 °C is implied for the Northern Hemisphere during this period of Late Cretaceous time. A remarkably similar figure of ~14 °C difference between low- and high-latitude surface water was computed for the late Maastrichtian of the Southern Hemisphere, based on oxygen-isotope ratios of well-preserved planktonic foraminifera[20].

The Maastrichtian calibration point allows a tentative Mid- to Late Cretaceous palaeotemperature curve for the Arctic Ocean to be generated using $\delta^{18}O$ data from other localities. Relatively long $\delta^{18}O$ time series exist for southern England (Chalk), central Italy (Scaglia: lithified pelagic limestone), Ocean Drilling Program Sites on the Exmouth plateau off western Australia (chalks and claystones) and in the Southern Ocean where species-specific planktonic and benthonic foraminifera have been analysed[21,22]. All these curves, whether or not derived from material that has been deeply buried and, in some cases, uplifted to experience possible meteoric-water diagenesis, show a remarkable similarity, demonstrating conclusively that the climatic trends are global in nature. The Cretaceous palaeotemperature profiles indicate, with some reversals, warming from the Albian through the Cenomanian, to peak either at Cenomanian–Turonian boundary time or in the early to middle Turonian, followed by a general decline through the Coniacian, Santonian and Campanian to reach a definitive minimum in the Maastrichtian. The smoothed curve from the English Chalk, taken to record broad temperature changes across the Northern Hemisphere, represents a composite record from outcrop

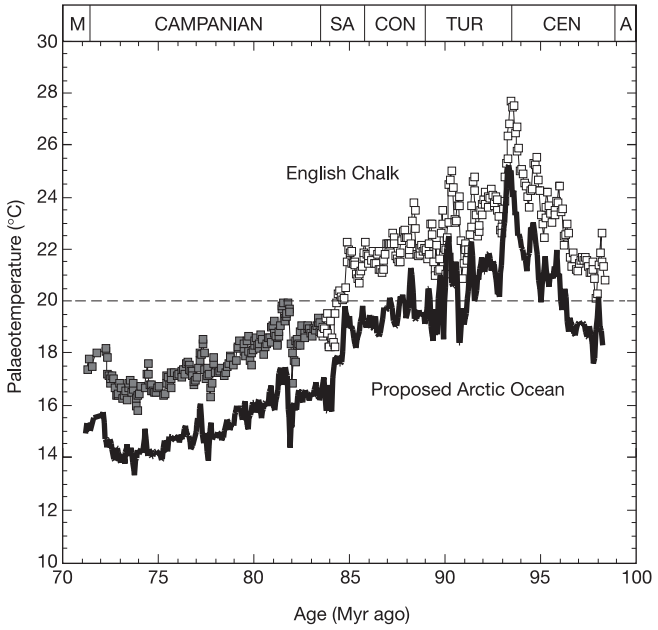

Figure 3 Proxy palaeotemperature curve for the Arctic Ocean. This curve (bold black line) is taken from oxygen-isotope ratios of bulk chalk from southern England (depositional palaeolatitude of ~40° N; ref. 31), calibrated against a value of 15 °C for the early Maastrichtian. Stratigraphic overlap in the lowest Campanian of the two curves (coastal outcrop in East Kent: unfilled squares) and borehole material in Norfolk (Trunch borehole: filled squares) permits adjustment of the $\delta^{18}O$ values, and hence calculated palaeotemperatures, of core samples. This adjustment is based on the assumption that the more lithified chalks record an additional burial diagenetic overprint: the core samples have consistently lower $\delta^{18}O$ values (by ~0.7‰) than coeval outcrop material. Palaeotemperatures on a smoothed (three-point moving average) curve are calculated using a standard formula, assuming a value of −1.0‰ SMOW for an ice-free Cretaceous ocean[21]. Note the 'tropical' polar climates (dashed line at 20 °C) attained during the Cenomanian and Turonian stages.

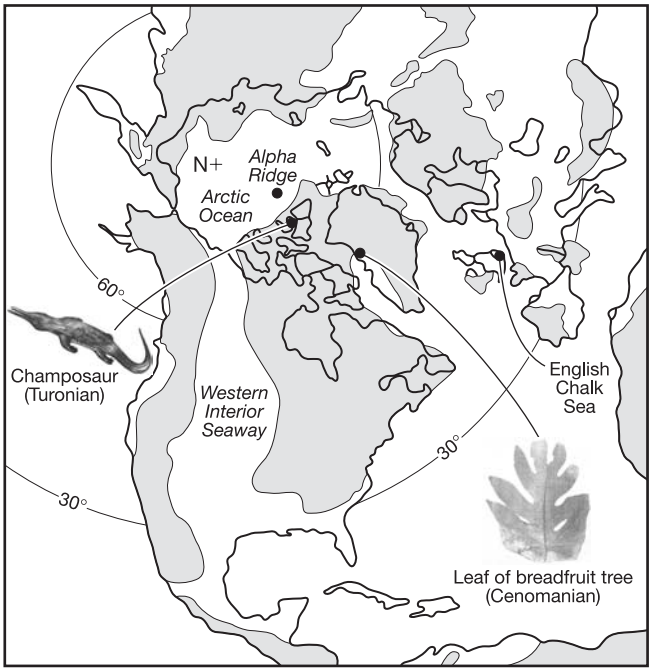

Figure 4 Northern Hemisphere view of the Arctic Ocean during the Late Cretaceous (Turonian). This projection shows the likely connections of the Arctic Ocean to epicontinental seas, such as that of the western interior of North America and the north European shelf[31]. Approximate location of English Chalk outcrops in southeast England also shown. Position of fossil remains of breadfruit-tree leaves (image of the actual specimen recovered shown) is after ref. 24. Position and image of champosaur are from refs 25 and 26, respectively. Approximate position of the Alpha ridge[2] indicates its relative proximity to land, as also suggested by the presence of abundant terrestrial material in the lower Maastrichtian black muds.

(East Kent) and core material (Trunch borehole, Norfolk) joined at a level of the lowest Campanian (Fig. 3). Smoothing may reduce the significance of real episodes of short-period high and low temperatures but equally helps to eliminate the influence of diagenetic artefacts produced in intervals where post-depositional calcite cements dominate the isotopic signature.

Because the chalk palaeotemperature curve extends into the lowest Maastrichtian, it can be applied to the Arctic Ocean using the value of 15 °C as a calibration point on the simplifying assumption that the latitudinal gradient did not greatly change over the time period in question. Using this proxy curve for the Arctic Ocean suggests average surface-water temperatures in excess of 20 °C during much of the Cenomanian–Turonian interval (Fig. 3). There is palaeontological evidence to support the notion of such warm balmy climates at the North Pole (Fig. 4). Fossil leaves and pseudo-fruit of the breadfruit tree *Artocarpus dicksoni*, whose present-day 'ultra-tropical' relatives grow in a temperature range of ~15–38 °C (ref. 23), were discovered as long ago as 1883 in Cenomanian sediments of western Greenland[24], and the skeletal remains of large crocodile-like champosaurs from the Turonian of the Canadian Arctic archipelago (western Axel Heiberg island, Fig. 1) imply a mean annual ambient temperature exceeding 14 °C (refs 25, 26). Interpretations from leaf physiognomy for the Turonian of the circum-Arctic region suggest somewhat lower temperatures[27]. Similar palaeobotanical studies on Cretaceous plant-bearing units on the north slope of Alaska, taken to suggest mean annual air temperatures at sea level of 5 °C in the Campanian–Maastrichtian[28], are incompatible with the results presented here, implying that all such physiognomic floral data need to be re-evaluated.

In conclusion, these warm Arctic marine palaeotemperatures are consistent with models of a CO_2-rich Cretaceous atmosphere characterized by a vigorous hydrological cycle[17]. Exactly how a mean annual marine temperature of 15 °C was resolved into seasonal variation is unknown, but this figure implies a total absence of polar ice at these high latitudes, and contrasts dramatically with a present-day mean annual surface air temperature of about −15 °C at 80° N (ref. 17). □

Methods

Powdered and freeze-dried sediments (1–3 g dry mass) were extracted with dichloromethane (DCM)/methanol (2:1) by using the Dionex accelerated solvent extraction technique. The extracts were separated by Al_2O_3 column chromatography using hexane/DCM (9:1), DCM/methanol (95:5) and DCM/methanol (1:1) as subsequent eluents to yield the apolar, tetraether and polar fractions, respectively. The apolar and desulphurized (using Raney Ni) polar fractions were analysed by gas chromatography and gas chromatography/mass spectrometry. The tetraether fractions were analysed as in ref. 6 except that separation was achieved on a Prevail Cyano column (2.1 × 150 mm, 3 μm, with flow rate at 0.2 ml min^{-1}), and single ion monitoring of the $[M + H]^+$ ions (dwell time, 234 ms) was used to identify the tetraether lipids with 1–4 cyclopentane rings (see ref. 6) and calculate the TEX_{86} values. These values were converted to sea surface temperature (SST) according to the equation:

$$TEX_{86} = 0.015SST + 0.29 \quad (1)$$

Equation (1) is updated from ref. 6, and is based on correlating TEX_{86} values of >60 core-top sediments with annual mean SSTs ranging between 0 and 28 °C. Replicate analysis has shown that the error in TEX_{86} values is ~0.01 or ~1 °C. This substantial improvement in analytical reproducibility (compare ref. 6) is mainly due to improved chromatographic conditions and the use of single-ion monitoring instead of a full scanning technique.

The high correlation of the TEX_{86} values with SST ($r^2 = 0.92$ for equation (1)) is in

agreement with the known physiological adaptation to temperature of the tetraether membrane lipid composition in cultured hyperthermophilic Archaea and their marine mesophilic descendants[29]. Previous studies have also shown that the TEX_{86} parameter is not sensitive to salinity or depositional redox conditions[29,30]. Furthermore, initial applications show that reconstructed SSTs for Cretaceous sediments agree well with those derived from oxygen-isotope ratios of pristine skeletal carbonate[16].

Bulk organic isotopes and TOC contents were determined by decalcifying powdered rock samples with 2 N hydrochloric acid and analysing the decalcified sediments in duplicate on a Carlo Erba 1112 Flash Elemental Analyser coupled to a Thermofinnigan Delta Plus isotope mass spectrometer. Analytical errors for TOC range from 0.3% to 2%, and for $\delta^{13}C_{org}$ (‰ versus VPDB) are <0.1‰.

Received 10 June; accepted 28 October 2004; doi:10.1038/nature03143.

1. Clark, D. L. Early history of the Arctic Ocean. *Paleoceanography* **3,** 539–550 (1988).
2. Clark, D. L., Byers, C. W. & Pratt, L. M. Cretaceous black mud from the central Arctic Ocean. *Paleoceanography* **1,** 265–271 (1986).
3. Mudie, P. J. & Blasko, S. M. in *Initial Geological Report on CESAR: The Canadian Expedition to Study the Alpha Ridge* (eds Jackson, H. R., Mudie, P. J. & Blasko, S. M.) 59–99 (Paper 84–22, Geol. Surv. Canada, Ottawa, 1985).
4. Firth, J. V. & Clark, D. L. An early Maastrichtian organic-walled phytoplankton cyst assemblage from an organic-walled black mud in Core Fl-533, Alpha Ridge: evidence for upwelling conditions in the Cretaceous Arctic Ocean. *Mar. Micropaleont.* **34,** 1–27 (1998).
5. Jokat, W. Seismic investigations along the western sector of Alpha Ridge, Central Arctic Ocean. *Geophys. J. Int.* **152,** 185–201 (2003).
6. Schouten, S., Hopmans, E. C., Schefuß, E. & Sinninghe Damsté, J. S. Distributional variations in marine crenarchaeotal membrane lipids: a new tool for reconstructing ancient sea water temperatures? *Earth Planet. Sci. Lett.* **204,** 265–274 (2002).
7. Gradstein, F. M. *et al.* A Mesozoic time scale. *J. Geophys. Res. B* **99,** 24051–24074 (1994).
8. Dell'Agnese, D. J. & Clark, D. L. Siliceous microfossils from the warm Late Cretaceous and Early Cenozoic Arctic Ocean. *J. Paleontol.* **68,** 31–47 (1994).
9. Stoffyn-Egli, P. Iron and manganese micro-precipitates with a Cretaceous biosiliceous ooze from the Arctic Ocean: possible hydrothermal source. *Geo-Mar. Lett.* **7,** 223–231 (1987).
10. Mudie, P. J. in *Initial Geological Report on CESAR: The Canadian Expedition to Study the Alpha Ridge* (eds Jackson, H. R., Mudie, P. J. & Blasko, S. M.) 148–174 (Paper 84–22, Geol. Surv. Canada, Ottawa, 1985).
11. Barron, J. A. in *Initial Geological Report on CESAR: The Canadian Expedition to Study the Alpha Ridge* (eds Jackson, H. R., Mudie, P. J. & Blasko, S. M.) 137–148 (Paper 84–22, Geol. Surv. Canada, Ottawa, 1985).
12. Bukry, D. in *Initial Geological Report on CESAR: The Canadian Expedition to Study the Alpha Ridge* (eds Jackson, H. R., Mudie, P. J. & Blasko, S. M.) 125–135 (Paper 84–22, Geol. Surv. Canada, Ottawa, 1985).
13. Sinninghe Damsté, J. S. *et al.* The rise of the rhizosolenid diatoms. *Science* **304,** 584–587 (2004).
14. Holba, A. G. *et al.* Application of 24-norcholestanes for constraining source ages of petroleum. *Org. Geochem.* **29,** 1269–1283 (1998).
15. Kitchell, J. A. & Clark, D. L. Late Cretaceous–Paleogene paleogeography and paleocirculation: evidence of north polar upwelling. *Palaeogeogr. Palaeoclimatol. Palaeoecol.* **40,** 135–165 (1982).
16. Schouten, S. *et al.* Extremely high sea-surface temperatures at low latitudes during the middle Cretaceous as revealed by archaeal membrane lipids. *Geology* **31,** 1069–1072 (2003).
17. Barron, E. J. A warm, equable Cretaceous: the nature of the problem. *Earth Sci. Rev.* **19,** 305–338 (1983).
18. Barrera, E. & Savin, S. M. in *Evolution of the Cretaceous Ocean–Climate System* (eds Barrera, E. & Johnson, C. C.) 245–282 (Spec. Paper 332, Geol. Soc. Am., Boulder, Colorado, 1999).
19. Wilson, P. A. & Opdyke, B. N. Equatorial sea-surface temperatures for the Maastrichtian revealed through remarkable preservation of metastable carbonate. *Geology* **24,** 555–558 (1996).
20. Huber, B. T., Hodell, D. A. & Hamilton, C. P. Mid- to Late Cretaceous climate of the southern high latitudes. Stable isotopic evidence for minimal equator-to-pole thermal gradients. *Bull. Geol. Soc. Am.* **107,** 1164–1191 (1995).
21. Jenkyns, H. C., Gale, A. S. & Corfield, R. M. Carbon- and oxygen-isotope stratigraphy of the English Chalk and Italian Scaglia and its palaeoclimatic significance. *Geol. Mag.* **131,** 1–34 (1994).
22. Clarke, L. J. & Jenkyns, H. C. New oxygen-isotope evidence for long-term Cretaceous climate change in the Southern Hemisphere. *Geology* **27,** 699–702 (1999).
23. Morton, J. F. *Fruits of Warm Climates* (Creative Resources Systems, Miami, 1987).
24. Nathorst, A. G. Ueber die Reste eines Brotfruchtbaums ARTOCARPUS DICKSONI N. SP., aus den cenomanen Kreideablagerungen Grönlands. *Kongl. Svenska Vetenskaps-Akad. Hand* **24,** 2–9 (1890).
25. Tarduno, J. A. *et al.* Evidence for extreme climatic warmth from Late Cretaceous Arctic vertebrates. *Science* **282,** 2241–2244 (1998).
26. Huber, B. T. Tropical paradise at the Cretaceous poles? *Science* **282,** 2199–2200 (1998).
27. Herman, A. B. & Spicer, R. A. Palaeobotanical evidence for a warm Cretaceous Arctic Ocean. *Nature* **380,** 330–333 (1996).
28. Spicer, R. A. & Parrish, J. T. Late Cretaceous–early Tertiary palaeoclimates of northern high latitudes: a quantitative view. *J. Geol. Soc. Lond.* **147,** 329–341 (1990).
29. Wuchter, C., Schouten, S. & Sinninghe Damsté, J. S. Temperature-dependent variation in the distribution of tetraether membrane lipids of marine Crenarchaeota: Implications for TEX_{86} paleothermometry. *Paleoceanography* (in the press).
30. Schouten, S., Hopmans, E. & Sinninghe Damsté, J. S. The effect of maturity and depositional redox conditions on archaeal tetraether lipid palaeothermometry. *Org. Geochem.* **35,** 567–571 (2004).
31. Hay, W. W., Eicher, D. L. & Diner, R. in *Evolution of the Western Interior Basin* (eds Caldwell, W. G. E. & Kauffman, E. G.) 297–318 (Spec. Pap. 39, Geol. Ass. Canada, St John's, Newfoundland, 1993).

Acknowledgements We thank D. Clark for indicating the whereabouts of core Fl-533, and T. Simo for locating it in the Department of Geology and Geophysics of the University of Wisconsin at Madison. S. Rampen and J. Ossebaar (Royal NIOZ) are thanked for analytical assistance.

Competing interests statement The authors declare that they have no competing financial interests.

Correspondence and requests for materials should be addressed to H.C.J. (hughj@earth.ox.ac.uk).

Recycling lower continental crust in the North China craton

Shan Gao[1,2], Roberta L. Rudnick[3], Hong-Ling Yuan[1], Xiao-Ming Liu[1], Yong-Sheng Liu[2], Wen-Liang Xu[4], Wen-Li Ling[2], John Ayers[5], Xuan-Che Wang[2] & Qing-Hai Wang[4]

[1]*Key Laboratory of Continental Dynamics, Department of Geology, Northwest University, Xi'an 710069, China*
[2]*Faculty of Earth Sciences, China University of Geosciences, Wuhan 430074, China*
[3]*Geochemistry Laboratory, Department of Geology, University of Maryland, College Park, Maryland 20742, USA*
[4]*School of Earth Sciences, Jilin University, Changchun 130061, China*
[5]*Department of Geology, Vanderbilt University, PO Box 105 Station B, Nashville, Tennessee 37235, USA*

Foundering of mafic lower continental crust into underlying convecting mantle has been proposed as one means to explain the unusually evolved chemical composition of Earth's continental crust[1,2], yet direct evidence of this process has been scarce. Here we report that Late Jurassic high-magnesium andesites, dacites and adakites (siliceous lavas with high strontium and low heavy-rare-earth element and yttrium contents) from the North China craton have chemical and petrographic features consistent with their origin as partial melts of eclogite that subsequently interacted with mantle peridotite. Similar features observed in adakites and some Archaean sodium-rich granitoids of the tonalite-trondhjemite-granodiorite series have been interpreted to result from interaction of slab melts with the mantle wedge. Unlike their arc-related counterparts, however, the Chinese magmas carry inherited Archaean zircons and have neodymium and strontium isotopic compositions overlapping those of eclogite xenoliths derived from the lower crust of the North China craton. Such features cannot be produced by crustal assimilation of slab melts, given the high Mg#, nickel and chromium contents of the lavas. We infer that the Chinese lavas derive from ancient mafic lower crust that foundered into the convecting mantle and subsequently melted and interacted with peridotite. We suggest that lower crustal foundering occurred within the North China craton during the Late Jurassic, and thus provides constraints on the timing of lithosphere removal beneath the North China craton.

Eclogite forms by high- to ultrahigh-pressure metamorphism of basaltic rocks and has a density that is higher than that of peridotite by 0.2–0.4 g cm^{-3} (ref. 3). Because of this density contrast, mafic lower continental crust (together with the underlying lithospheric mantle) can be recycled into the mantle when granulite is transformed into eclogite during crustal thickening[1,4]. Such foundering may explain collapse of mountains, basin formation and associated magmatism, which is generated by asthenospheric upwelling into the space previously occupied by thickened lithosphere[5]. Density foundering may also explain the absence of high-pressure mafic residues that are the complement to the voluminous tonalite-